GEOPHYSICS, VOL. 71, NO. 6 (NOVEMBER-DECEMBER 2006); P. L75–L86, 15 FIGS., 3 TABLES.
10.1190/1.2345192

Automatic inversion of magnetic anomalies from two height levels using finite-difference similarity transforms

Petar Stavrev[1], Daniela Gerovska[2], and Marcos J. Araúzo-Bravo[3]

ABSTRACT

We solve the inverse magnetic problem for the depth and shape of simple sources in the presence of a regional field and truly random noise. We do not use noise-generating derivatives nor are we forced to solve complex systems of equations. Our inverse operator applies a new geometric type of field transform, the finite-difference similarity transform (FDST), that is based on a postulated degree of homogeneity in the potential field. Magnetic data from two height levels are required for the calculation of the FDSTs. The FDSTs are generated for an assumed central point of similarity (CPS) and a trial value (index) for the coefficient of similarity, and they are sensitive to the distance between the source and the CPS and to the agreement between the index and the degree of homogeneity in the data. When the CPS converges to a singular point in the potential field, say, the center or the top edge of the source, and when the trial index converges on the degree of homogeneity present in the data, the FDST drops in amplitude and its plot approaches a straight line, thereby signaling an interpretation for the source position and type. All inverse operations are fully automated and applicable to the interpretation of large data sets. The necessary data for the second level can be obtained by actual measurement or, alternatively, by deriving them from the data at the first level by an upward, analytical continuation. Upward continuation suppresses high-wavenumber random noise and thus contributes to a stable inversion. Model tests show that a suitable height for the second level is less than the expected depth of the source below the first level, while a suitable window length is about twice that depth. Examples show that the proposed inversion is effective on both model and field data. Note that this approach can be extended to the inversion of any component or derivative of the 2D or 3D magnetic or gravity fields from simple sources.

INTRODUCTION

Modern magnetic and gravity data acquisition produces large data sets that require efficient, automatic inversion methods. This automation is achieved through procedures that use minimum additional information, simplified interpretation models with one or two singular points, and unified algorithms for inversion of different model types. In this respect, a useful common property of potential fields from simple sources is their homogeneity, which serves as a theoretical basis for many known automatic or semiautomatic inversion techniques that follow the principal articles of Thompson (1982) and Reid et al. (1990). The method proposed here is also based on the homogeneity property of magnetic anomalies.

The homogeneity of a function is expressed in two forms. First, it is expressed through the principal definition of a homogeneous function by the equation (Courant and John, 1965)

$$f(t\nu_1,\ t\nu_2,\ \ldots, t\nu_i,\ \ldots, t\nu_j) = t^n f(\nu_1, \nu_2,\ \ldots,\ \nu_i,\ \ldots,\ \nu_j), \qquad (1)$$

where $\boldsymbol{\nu} = (\nu_1, \nu_2, \ldots, \nu_i, \ldots, \nu_j)$ is the set of variables with respect to which the function f shows the homogeneity, t is a coefficient, and n is the degree of homogeneity. Differentiate equation 1 with respect to t and set t equal to unity to obtain Euler's partial differential equation for homogeneous functions,

Manuscript received by the Editor December 28, 2004; revised manuscript received February 17, 2006; published online October 23, 2006; corrected version published online October 27, 2006.
[1]University of Mining and Geology, Department of Applied Geophysics, 1700 Sofia, Studentski grad, Bulgaria. E-mail: stavrev@mgu.bg.
[2]Kyushu University, Department of Earth Resources Engineering, Laboratory of Geothermics, Hakozaki 812-8581, Fukuoka, Japan. E-mail: gerovska_daniela@hotmail.com.
[3]Kyushu Institute of Technology, Department of Biosciences and Bioinformatics, Faculty of Computer Science and Systems Engineering, Iizuka 820 8502, Japan. E-mail: mararabra@yahoo.co.uk.

$$\nu_1\frac{\partial f}{\partial \nu_1} + \nu_2\frac{\partial f}{\partial \nu_2} + \cdots + \nu_i\frac{\partial f}{\partial \nu_i} + \cdots + \nu_j\frac{\partial f}{\partial \nu_j} = nf(\nu_1, \nu_2, \ldots, \nu_i, \ldots, \nu_j). \quad (2)$$

If a function satisfies Euler's equation 2, it also satisfies equation 1, and vice versa (Courant and John, 1965).

The property of homogeneity finds applications in the inverse magnetic and gravity problems in two principal approaches, corresponding respectively to equations 1 and 2. The first, more popular of the two is the approach based on Euler's differential equation 2. Thompson (1982) proposed an automated method to estimate the source's depth, type, and constant background as a 2D linear inverse problem for magnetic models with one singular point. The source type is determined by the degree of homogeneity n, which taken with a negative sign gives the structural index $N = -n$. This method was extended for 3D problems by Reid et al. (1990) and described as Euler deconvolution. In the traditional implementation of Euler deconvolution, the structural index takes on a series of prescribed values. The estimated depth is the solution to an overdetermined system of linear equations 2 that displays minimal dispersion. Methods for obtaining a solution without prescribing a structural index have also been proposed (Slack et al., 1967; Stavrev, 1997; Hsu, 2002; Keating and Pilkington, 2004; Gerovska et al., 2005). The instability of the solutions for the depth and structural index remains a major problem of Euler deconvolution (Reid, 1995; Ravat, 1996). This is an ill-posed problem (Barbosa et al., 1999) like most of the inverse potential-field problems. The main reason for the instability is the high correlation coefficient between the anomalies ΔT and their vertical derivative $\partial\Delta T/\partial z$. This causes coupling effects between N and z_0 as unknowns associated with the coefficients ΔT and $\partial\Delta T/\partial z$, respectively, in the system of Euler's equations 2. The problem can be solved by employing additional information and using regularization operators (Tikhonov and Arsenin, 1977) or applying other strategies based on clustering of large sets of unstable solutions (Gerovska and Araúzo-Bravo, 2003; Mikhailov et al., 2003; Keating and Pilkington, 2004).

The second, less popular approach is based on the direct application of equation 1, and we may mention it for the solutions obtained by wavelet transforms (Moreau et al., 1997) and by similarity transforms (Stavrev, 1997). The use of homogeneity expressed by equation 1 does not involve differential equations in the inverse procedures. The inversion technique proposed here also uses equation 1. The method is based on a comparison between the similarly transformed field and the original field given on at least two levels of measured or upward continued field. The numerical result from their subtraction is the finite-difference similarity transform (FDST). The horizontal location, depth, and type of the source are estimated without using derivatives and systems of equations. The method has inherent possibilities for the elimination of constant or linear background and the suppression of random noise. An implementation of this method in a fully automatic way is described later. Several synthetic examples and two field applications illustrate the principal concept and efficiency of the proposed automatic inverse procedures.

THEORETICAL CONSIDERATIONS

Homogeneity of simple interpretation models

For the elementary interpretation models with one singular point $M(x_0, y_0, z_0)$, equations 1 and 2 take on their simplest form. A suitable example to illustrate this form is the 2D model of a thin magnetic dike with its top at a point $M(x_0, z_0)$ and infinite depth extent. The analytical expression of the total magnetic anomaly (TMA) ΔT caused by such a source (e.g., Telford et al., 1990) is

$$\Delta T = 2Jw\frac{s(x_0 - x) + l(z_0 - z)}{(x_0 - x)^2 + (z_0 - z)^2}, \quad (3)$$

where $(z_0 - z)$ is the depth to the dike top M when the z-axis is positive vertically downward; $w \ll (z_0 - z)$ is the thin dike width; $l = \cos\Theta\sin I_0 - \sin\Theta\cos I_0\cos(D_p - D_0)$; $s = \sin\Theta\sin I_0 - \cos\Theta\cos I_0\cos(D_p - D_0)$; $\Theta = \alpha - \varphi$ is the difference between the dip angle α of the dike and the dip angle φ of the vector $\mathbf{J}$ of the effective magnetization; D_p is the geographic azimuth of the 2D magnetic profile; and I_0 and D_0 are the inclination and declination of the geomagnetic field, respectively. The well-known result for the homogeneity of expression 3 is $n = -1$, which gives $N = 1$ (e.g., Thompson, 1982). The same result can be obtained by using equation 1 if the distance or all coordinates are multiplied by the coefficient t:

$$\Delta T(tx, tz, tx_0, tz_0) = 2Jw\frac{s(tx_0 - tx) + l(tz_0 - tz)}{(tx_0 - tx)^2 + (tz_0 - tz)^2} = t^{-1}\Delta T(x, z, x_0, z_0). \quad (4)$$

Clearly, equation 4 shows the transformed field $\Delta T(tx, tz, tx_0, tz_0)$ is defined at points with coordinates (tx, tz) and has as its equivalent source a dike with a top at a point with coordinates (tx_0, tz_0). The quantities $J, w, \Theta, \alpha, \varphi, D_p, I_0$, and D_0 remain unchanged. This analysis of equation 4 shows that equation 1 for potential fields may have a completely determined physical sense. The geometric and physical interpretation of equation 1 for potential fields is the theoretical basis of some inversion techniques described below.

An expression that follows directly from equation 1 is (Courant and John, 1965)

$$f(\boldsymbol{\nu}) = \nu_i^n f_i\left(\frac{\nu_1}{\nu_i}, \frac{\nu_2}{\nu_i}, \cdots, \frac{\nu_j}{\nu_i}\right), \quad (5)$$

where an element ν_i from the set $\boldsymbol{\nu}$ is chosen as a denominator. For example, the analytical expression 3 allows the following representation:

$$\Delta T = 2Jw(z_0 - z)^{-1}\frac{s\dfrac{x_0 - x}{z_0 - z} + l}{\left(\dfrac{x_0 - x}{z_0 - z}\right)^2 + 1} = 2Jw\frac{1}{z_0 - z}\frac{sq + l}{q^2 + 1}, \quad (6)$$

where the chosen denominator $(z_0 - z)$ appears with an exponent equal to -1, thus showing a degree of homogeneity $n = -1$, according to equation 5. The dimensionless argument in the right side of equation 6 is the ratio $q = (x_0 - x)/(z_0 - z)$. As q has a constant value for different observation levels $z = z_i$, i.e., if $q = (x_0 - x_i)/(z_0 - z_i) = \text{const}$, it defines a straight line $x_i = x_0 - q(z_0 - z_i)$ through the dike top $M(x_0,z_0)$ with an angular coefficient q. The product $(z_0 - z_i)^n \Delta T(q)$ remains a constant along this line. If at least two such lines can be drawn, then their intersection indicates the top $M(x_0,z_0)$ of the dike. The other types of singular points also allow such localization.

The above-mentioned property has found applications in the methods based on wavelet transforms (Moreau et al., 1997). Analytical continuations of the anomalous field to a series of heights z_i above the observation level may be calculated for the purpose. In terms of the wavelet method, the height of the analytical continuation is the dilation parameter in the dilation operator of the continuous wavelet transform. The latter is a convolution of the dilation operator and the potential field, according to Poison's integral. In a 2D case, the dilation operator in the integral expression has the form $(1/\pi)[1/(z' - z)][1/(q^2 + 1)]$, where (x',z') are coordinates of points at the original field observation level, (x,z) are the coordinates of the points where the wavelet transform is calculated, $(z' - z) = a$ is the dilation parameter, and $q = (x' - x)/(z' - z)$ is a dimensionless quantity that determines the analyzing wavelet $\psi = (1/\pi)[1/(q^2 + 1)]$. This structure of the dilation operator shows a treatment of Poison's semigroup kernel as a homogeneous function, represented in form 5.

We should note that expression 6 of the ΔT anomaly for a dike has a similar structure. Therefore, the approach using equation 5, definition 1, in the wavelet inverse method has the property of homogeneity as its natural basis. This approach was extended for the case of anomalous fields with two or more singular points (Martelet et al., 2001; Sailhac and Gibert, 2003). An alternative technique was proposed by Vallée et al. (2004) using wavelet transforms of up to the second order.

The problem with multipolar models is the deviation of the lines of maxima of wavelet transforms from the strongly straight lines near the singular points. This problem has been studied analytically and numerically by Dimitrov and Stavrev (1968), although not in terms of wavelet transforms at that time, but in terms of deviations, or systematic errors, from the straight lines depending on the level of the analytical continuation and the ratio q. Optimal continuation levels and ratios have been found for the magnetic models of a thin and a thick dike and for the gravity and magnetic models of a thin 2D horizontal plate of finite width.

Similarity transforms

The similarity transform used in the affine geometry (e.g., Gellert et al., 1979) can be applied to magnetic fields described as space phenomena. This transform is a geometric transform with respect to a CPS chosen at a point $C(a,b,c)$ in a Cartesian coordinate system. For a given coefficient of similarity $t > 0$ and a parameter u, the similarity transform ΔT^* of a TMA ΔT has the expression

$$\Delta T^*(x^*,y^*,z^*) = t^u \Delta T(x,y,z), \tag{7}$$

where

$$x^* = a + t(x - a), \quad y^* = b + t(y - b), \quad z^* = c + t(z - c). \tag{8}$$

Figure 1 illustrates a simple example for a similarity transform (ST) of a TMA ΔT caused by a 2D line of dipoles. The observation points $P(x,0)$ are located along the horizontal x-axis of a Cartesian coordinate system with the z-axis positive downward. The CPS coincides with the coordinate system origin, i.e., $a = 0$ and $c = 0$. In this case, the similar images $P^*(x^*,z^*)$ of the points $P(x,0)$ are distributed along the same x-axis because, according to equation 8, $x^* = tx, z^* = tz = 0$. The three curves ΔT^* (Figure 1a) correspond to three different values of the parameter u for the same coefficient $t = 1.5$. The calculated STs, ΔT^*, can be physically interpreted as anomalies of the geometric similarity transformed source B^* of the original source B (Figure 1b), with a ratio between their magnetic moments per unit length $\boldsymbol{\mu}^*$ and $\boldsymbol{\mu}$, respectively, depending on the parameter u in equation 7. This physical interpretation follows the homogeneity of equation 1 and the analysis of equation 4.

For a simple magnetic model with one singular point $M(x_0,z_0)$, the homogeneity property of the TMA is expressed by

$$\Delta T(x^*,z^*,x_0^*,z_0^*) = t^n \Delta T(x,z,x_0,z_0), \tag{9}$$

where n is the degree of homogeneity and t is a coefficient; all $(^*)$ coordinates are determined according to equations 8. Equation 9 expresses a full geometric similarity transform of observation points and sources. The physical parameter $\mathbf{p}$ of the source B does not appear as a variable in expression 9. This means that it preserves its value and direction as a magnetic parameter of the geometrically transformed source B^*, i.e., $\mathbf{p}^* = \mathbf{p}$. The latter equality allows definition 7 for a parameter $u = n$ to be interpreted in the same way. Here, we

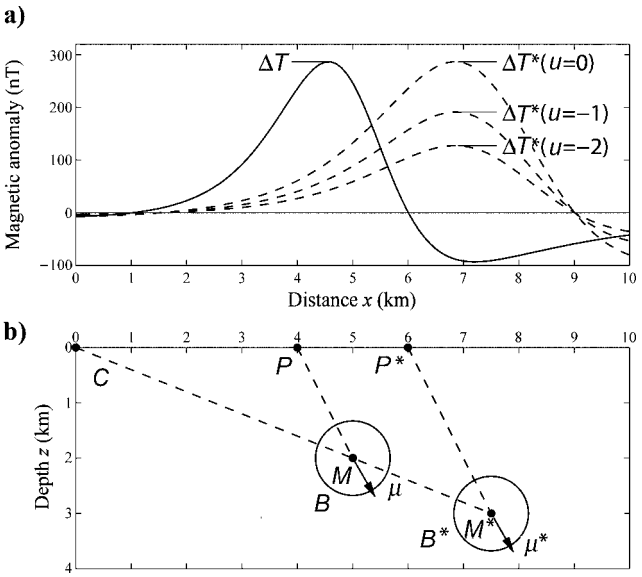

Figure 1. (a) Two-dimensional STs of a TMA ΔT caused by a line of dipoles or an equivalent horizontal cylinder; u is the parameter of STs at a coefficient of similarity $t = 1.5$; (b) vertical cross section of the 2D original source B at point M and its similar image B^* at point M^*. The CPS is chosen at the origin of the coordinate system; P^* is the similar image of one original observation point P; μ and μ^* are the physical parameters magnetic moment per unit length for the original and similarly transformed dipole line, respectively.

treat the parameter u as an unknown quantity that differs from the degree of homogeneity n by $\delta = u - n$. Then, according to equations 7–9, in a 2D case we have

$$\Delta T^*(x^*,z^*,x_0^*,z_0^*) = t^\delta \Delta T(x^*,z^*,x_0^*,z_0^*). \quad (10)$$

Hence, the difference δ affects the amplitude of ST, ΔT^*, with the multiplier t^δ. This effect is equivalent to a change of the physical parameter $\mathbf{p}^*$ with respect to the original parameter $\mathbf{p}$, so that

$$\mathbf{p}^* = t^\delta \mathbf{p} = t^{(u-n)}\mathbf{p}. \quad (11)$$

Thus, the choice of the parameter u controls the transfer of physical parameters from B to the similar virtual source B^*. The physical parameter $\mathbf{p}$ for the model of a line of dipoles is the magnetic moment per unit length: For the dike model, $\mathbf{p}$ is the product of the magnetization and the width of the thin dike; for the contact model, $\mathbf{p}$ is the magnetization vector. In the rest of this article, instead of the homogeneity degree n, we will use the more popular structural index $N = -n$ (Thompson, 1982). This index is $N = 2$ for the model of a line of dipoles (and the equivalent cylinder), $N = 1$ for the model of a semiinfinite sheet (and the equivalent thin dike, sill, and small step), and $N = 0$ for the contact model, e.g., (Reid et al., 1990).

Finite-difference similarity transforms

The FDST is defined as the difference D between the similarity transform $\Delta T^*(P^*)$ from equation 7 and the original field $\Delta T(P^*)$, measured or analytically continued, at the same points $P^*(x^*,z^*)$:

$$D(x^*,z^*) = \Delta T^*(x^*,z^*,x_0^*,z_0^*) - \Delta T(x^*,z^*,x_0,z_0). \quad (12)$$

In light of the physical meaning of the STs, the difference $D(P^*)$ can be considered as a difference between the anomalous fields of two sources. These are the similar virtual source B^* with a physical parameter $\mathbf{p}^* = t^{u+N}\mathbf{p}$ (see equation 11 for $n = -N$), and the original source B with the physical parameter $\mathbf{p}$. Another equivalent interpretation of the FDST as a sum of two fields is possible if we refer the minus sign in equation 12 to the physical parameter of the original source. Figure 2 illustrates the constituent elements of the FDST for the model of a thin dike with infinite depth extent. The model anomaly ΔT is calculated at points $P(x,z)$ at a level z = const (Figure 2b). The CPS at point $C(a,c)$ is chosen near the original source B, whose top is at point $M(x_0,z_0)$ (Figure 2b). The similarly transformed anomaly ΔT^* (Figure 2a) is calculated at a level z^* = const with a coefficient $t = (c - z^*)/(c - z)$. Its source is the similar body B^* of the dike with a top at the point $M^*(x_0^*,z_0^*)$, given by equations 8. The parameter $u = -1$ corresponds to the structural index $N = 1$ of the dike model. The minimum and the maximum of the curve D so obtained (Figure 2a) reflect the positions of the sources, original and virtual, respectively.

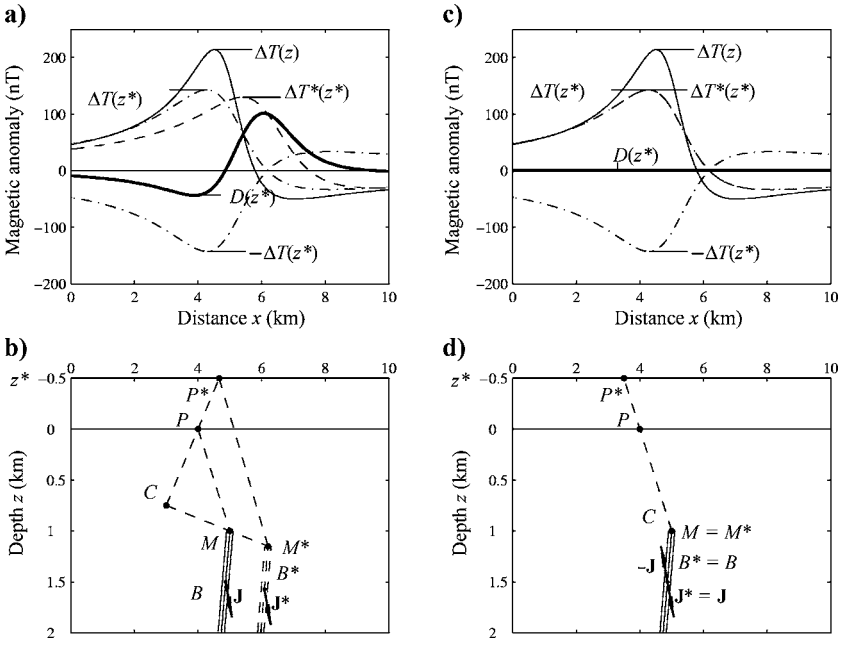

Figure 2. (a) Two-dimensional TMAs $\Delta T(x,z)$ at a level z and $\Delta T(x,z^*)$ at a higher level z^* caused by a thin dike with infinite depth extent; $\Delta T^*(x^*,z^*)$ is the similarity transform of $\Delta T(x,z)$ to the level z^*; D is the resultant curve of the FDST between $\Delta T^*(x^*,z^*)$ and $\Delta T(x^*,z^*)$. The parameter $u = -1$ corresponds to the structural index $N = 1$ of the dike model, and $t = 1.6667$ corresponds to $c = 0.75$. (b) Vertical cross section of the 2D thin dike B with top at point M and the similar dike B^* with top at point M^*. The chosen CPS at point $C(a,c)$ with $c > z$ generates similar images of observation points P at points P^* at level z^*; $\mathbf{J}$ and $\mathbf{J}^*$ are the magnetization vectors of the original B and similar B^* dikes, respectively. (c) The TMAs $\Delta T(x,z)$ and $\Delta T(x,z^*)$, given in (a), and the similar transform $\Delta T^*(x^*,z^*) = \Delta T(x^*,z^*)$ that yields an FDST curve $D(x^*,z^*) = 0$ because of the special position of the CPS shown in (d). (d) Vertical cross section of the original model source B and its similar image $B^* = B$ at $M^* = M$ when CPS coincides with the top point M of the original source.

FDST sensitivity to the CPS position

A change in the position of the CPS affects the distance between the sources B and B^*. In the 2D case of point sources, this distance R is defined by the expression

$$R = ((x_0^* - x_0)^2 + (z_0^* - z_0)^2)^{1/2}$$
$$= (t-1)((a - x_0)^2 + (c - z_0)^2)^{1/2}, \quad (13)$$

where (x_0,z_0) and (x_0^*,z_0^*) are the coordinates of field singular points coinciding with the characteristic points M and M^* of the sources B and B^*, respectively. Here the coordinates (x_0^*,z_0^*) are substituted by (x_0,z_0), according to equations 8. Clearly, the distance R decreases if we move the CPS $C(a,c)$ toward the point $M(x_0,z_0)$. By physical arguments, this decreases the difference D between the anomalies of the two sources. If the CPS $C(a,c)$ coincides with the point $M(x_0,z_0)$, then according to equation 13, $R = 0$. In this case, the two sources coincide geometrically. If the parameter u is selected so as to make their physical parameters $\mathbf{p}^* = \mathbf{p}$, then the difference of their anomalous fields is $D = 0$. This dependence of the FDST amplitudes on the CPS position is illustrated in Figures 2 and 3a for the model of a dike with infinite depth extent and in Figure 3b for the model of a horizontal cylinder (line of dipoles). Figure 2b and d shows the dike source geometry and its similar images at two different CPS positions, while Figure 2a and c represents the FDST

response for $u = -1$, i.e., for $N = 1$, which is the correct value for the structural index of the dike model. Figure 3a shows the monotonic changes of FDST amplitudes when the CPS approaches the dike top along a vertical line passing through it. Figure 3b illustrates the monotonic change in the FDST amplitudes for the line-of-dipoles model when the CPS approaches the source point M, following the horizontal line through this point.

Effect of finite source size

In real inverse problems, the sources have finite dimensions that are reflected in the FDST curves. When the depth extent of a dike or a contact is large but finite, the FDST values do not become zero but do present a straight-line profile over the source when the CPS coincides with the shallow singular point of the source field. Figure 4 shows this effect on the FDST for the model of a thin dike with large depth extent. The same effect of linearization of the FDST generated from the CPS coinciding with the upper edge point of a contact model is shown in Figure 5. As can be seen from Figures 4d and 5d, the equivalent source of the FDST is the part of the similar source body B^* that does not coincide with the original body B. For the common part of the two bodies B and B^*, the effective magnetization is $\mathbf{J}_e = \mathbf{J}^* + (-\mathbf{J}) = 0$. Where B^* does not coincide with B, $\mathbf{J}_e = \mathbf{J}^* - 0 = \mathbf{J}^*$, thus creating an anomalous effect. This part of B^* is below the lower source point M_2, so it has a significant depth and its equivalent field is weak and smooth, approximating a straight line along the observation profile (Figures 4c and 5c).

Effect of a linear background

The similarity transform of a linear function $\Phi = \alpha + \beta x + \gamma z$ is $\Phi^* = t^u \Phi$, which is a linear function of (x^*, z^*) following equations 8. If the magnetic profile $F = \Delta T + \Phi$ contains a linear background Φ, then at CPS, coinciding with the characteristic point of the source, the FDST of ΔT vanishes. Thus, the result for the FDST of data F contains only the linear effect because of the background Φ. Figure 6 shows the calculated FDST curves for the model of a thin dike in the presence of a linear background.

Suppression of high-wavenumber noise

The FDST may be generated as the difference between the similarity transform of the data and the upward continuation of the same data. Upward continuation applies a low-pass filter to both the signal and the noise. The similarity transform 7 does not, so some portion of the high-spatial-

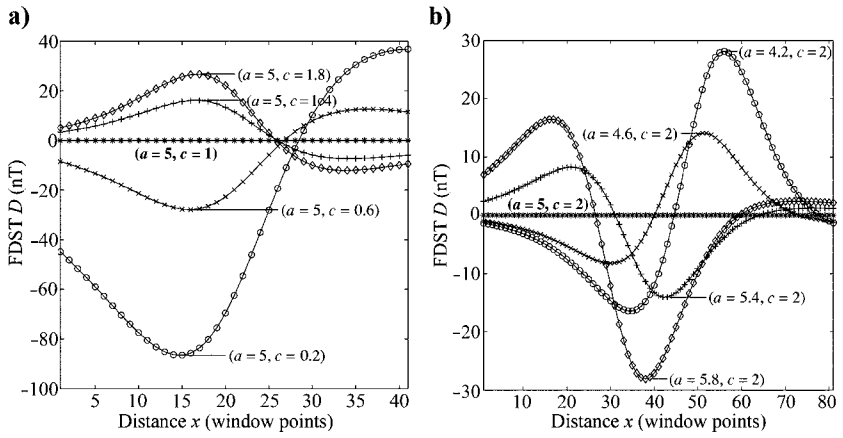

Figure 3. FDST curves D within one window for the model of (a) a dike with infinite depth extent (see Figure 2) for different CPS $C(a = 5$ km, $c = [0.2;0.6;1;1.4;1.8]$ km) along a vertical line through the characteristic point of the source with coordinates ($x_0 = 5$ km, $z_0 = 1$ km). The 41-point window, point spacing $dx = 0.1$ km, is centered over the dike characteristic point; (b) a horizontal cylinder (see Figure 1) with a characteristic point at ($x_0 = 5$ km, $z_0 = 2$ km) for different CPS $C(a = [4.2;4.6;5;5.4;5.8]$ km, $c = 2$ km) along a horizontal line through the characteristic point of the source. The 81-point window with $dx = 0.1$ km is centered over the respective CPS.

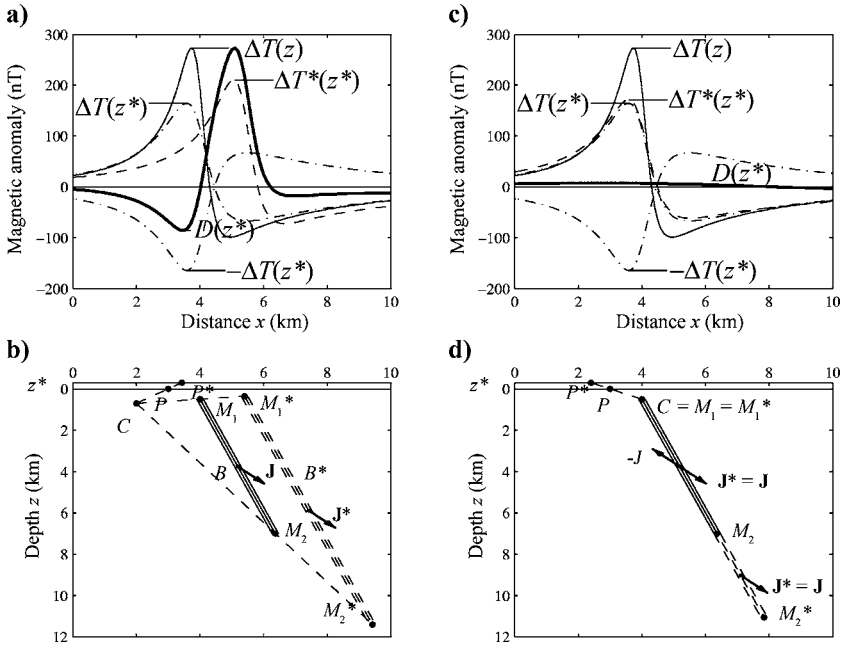

Figure 4. (a) Two-dimensional TMAs $\Delta T(x,z)$ at a level z and $\Delta T(x,z^*)$ at a higher level z^* caused by a thin dike with finite depth extent; $\Delta T^*(x^*,z^*)$ is the similarity transform of $\Delta T(x,z)$ to the level z^*; D is the resultant curve of the FDST between $\Delta T^*(x^*,z^*)$ and $\Delta T(x^*,z^*)$. The parameter $u = -1$ corresponds to the structural index $N = 1$ of the dike model, $t = 1.4286$. (b) Vertical cross section of the 2D thin dike B with top at point M_1 and lower edge at point M_2. The CPS at point C generates the similar image B^* of the dike with top at point M_1^* and lower edge at point M_2^*, and similar images of observation points P at points P^* at level z^*; $\mathbf{J}$ and $\mathbf{J}^*$ are the magnetization vectors of the original B and similar B^* dikes, respectively. (c) The TMAs $\Delta T(x,z)$ and $\Delta T(x^*,z^*)$ given in (a), and the similar transform $\Delta T^*(x^*,z^*)$ from CPS coinciding with the upper edge point M_1 of the dike. The FDST curve $D(x^*,z^*)$ is nearly a straight line and approximates the anomaly caused by the deeper dike with top at point M_2 shown in (d). (d) Vertical cross section of the model source B and its similar image $B^* = B$ when CPS coincides with the top point M_1 of the original source. The residual dike between edge points M_2 and M_2^* is the equivalent source of the FDST.

frequency noise remains in the difference. It may be reduced if an intermediate upward ($h_i < h$) continuation is used as input to the similarity transform.

FDST dependence on the choice of parameter *u*

The coincidence of a CPS with the characteristic source point is a necessary but insufficient condition for the FDST to approach a straight line. The other necessary condition is the equality of the physical parameters of the original body and the respective similar body. It depends on whether the choice of the parameter u of the ST (equation 7) is in agreement with the structural index N of the source. The FDST response to an incorrectly assigned N is illustrated in Figure 7 for a dike model with large depth extent. These synthetic tests show that the FDST cannot be reduced to a linear function for a wrong structural index.

From the analytical considerations and model examples above, we can conclude that the FDST is also sensitive to the position of its CPS relative to the source position. The coincidence of a CPS with the characteristic point of a point source is indicated by the FDST approaching zero or a straight line only when the chosen parameter u corresponds to the source type. Therefore, we propose an inversion technique whose main procedure is the search for a CPS position and for a parameter $u = -N$ that produce an FDST profile that is nearly a straight line.

METHOD

The setting for the implementation of the proposed inversion in the 2D case is shown in Figure 8. The TMA $\Delta T(x,z)$ is given at a level z, and its analytical continuation $\Delta T(x,z^*)$ is calculated at the level $z^* = z - h$, where h is the continuation height. The similarity transforms $\Delta T^*(x^*,z^*)$ within the frame of a given window W^* are generated from CPS $C(a,c)$, distributed along the vertical line through the window's midpoint. The CPS is like a set of probe points, imitating a vertical magnetic sounding in a search in depth for a straight-line FDST. The ST ΔT^* at the regular grid point P^* is equal to the interpolated ΔT value at the intermediate point $P(x,z)$ multiplied by t^u, according to equation 7. In this case, the coefficient of similarity is

$$t = \frac{\underline{CP^*}}{\underline{CP}} = \frac{c - z^*}{c - z}, \tag{14}$$

where $\underline{CP^*}$ and $\underline{CP}$ are the distances between the CPS C and the points P^* and P, respectively. The parameter u is prescribed a value between 0 and −2 (not necessarily an integer), corresponding to a structural index between 0 and 2. Thus, the FDST curve is calculated at all regular points P^* of the window W^*, according to equation 12. Each FDST curve $D(x^*,z^*)$, generated from a given CPS $C(a,c)$, is characterized by its proximity to a straight line within the frame of the window W^*. This property is estimated by the modulus of the residual standard deviation RSD* of $D(x^*,z^*)$ about its linear regression, i.e., by

$$\left|\mathrm{RSD}^*\right| = \left(\frac{\sum_{i=1}^{m} (D(x_i') - r_0 - r_x x_i')^2}{m - 2} \right)^{1/2}, \tag{15}$$

where m is the number of points within the window, W^*, $x_i' = (x_i^* - x_c^*)$ is the relative abscissa of points P^* with respect to the abscissa x_c^* of the midpoint of the window W^*, and r_0 and r_x are the regression coefficients

$$r_0 = \frac{\sum_{i=1}^{m} D(x_i')}{m},$$

$$r_x = \frac{\sum_{i=1}^{m} D(x_i' - r_0)x_i'}{\sum_{i=1}^{m} x_i'^2}. \tag{16}$$

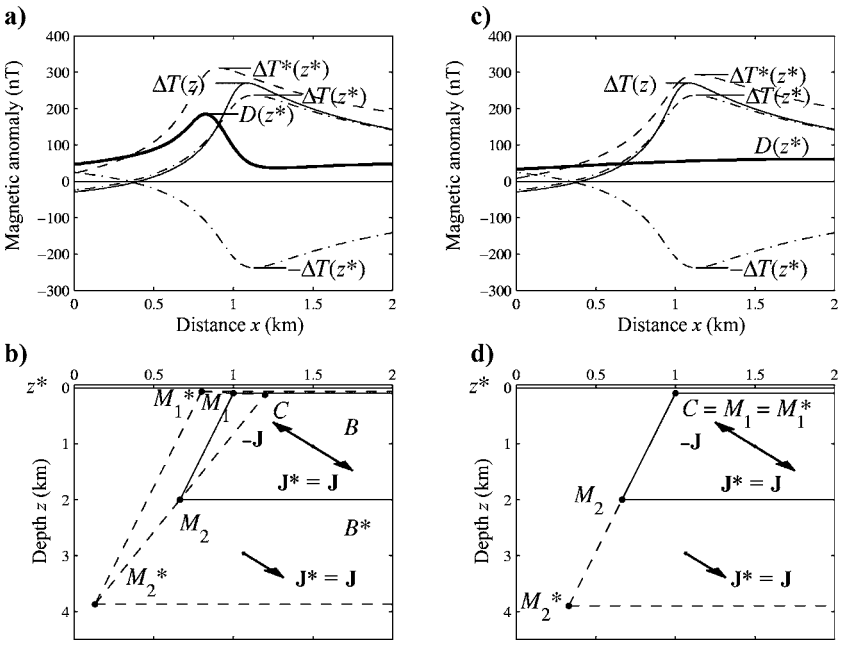

Figure 5. (a) 2D TMAs $\Delta T(x,z)$ at a level z and $\Delta T(x,z^*)$ at a higher level z^* caused by a contact with finite depth extent; $\Delta T^*(x^*,z^*)$ is the similarity transform of $\Delta T(x,z)$ to the level z^*; $D(x^*,z^*)$ is the resultant curve of FDST between $\Delta T^*(x^*,z^*)$ and $\Delta T(x^*,z^*)$. The parameter $u = 0$ corresponds to structural index $N = 0$ of contact model, $t = 1.3846$. (b) Vertical cross-section of the 2D thick contact B with upper edge at point M_1 and lower edge at point M_2. The CPS at point C generates the similar image B^* of the contact with upper edge at point M_1^* and lower edge at point M_2^*, and similar images of observation points P at points P^* at level z^*; $\mathbf{J}$ and $\mathbf{J}^*$ are the magnetization vectors of the original B and similar B^* contacts, respectively. (c) The TMAs $\Delta T(x,z)$ and $\Delta T(x^*,z^*)$ given in (a), and the similar transform $\Delta T^*(x^*,z^*)$ from CPS coinciding with the upper edge point M_1 of the contact. The FDST curve $D(x^*,z^*)$ is nearly a straight line and approximates the anomaly caused by the deeper contact with upper edge point M_2 shown in (d). (d) Vertical cross-section of the original model source B and its similar image $B^* = B$ when CPS coincides with the upper edge point, M_1, of the original source. The residual dike between edge points M_2 and M_2^* is the equivalent source of the FDST.

Here, we use a RSD^* normalized with the coefficient t, and relative to the RSD of the original data, dimensionless estimator of linearity

$$Q(a,c,u) = \frac{\frac{|RSD^*|}{|RSD|}}{t-1}, \qquad (17)$$

where $|RSD|$ is calculated according to equation 15 for the anomaly $\Delta T(x,z)$. The relative standard deviation increases Q for the noninformative, near-straight-line parts of the magnetic profile within the frame of the window W. The denominator $(t-1)$ increases Q for the CPS deeper than the characteristic point of the source, where the coefficient of similarity t obtains comparatively low values close to unity (see equation 14) and $(t-1)$ tends to zero. Around and at the singular point, where $|RSD^*| \le |RSD|(t-1)$, the estimator Q obtains values less than 1 (see Figures 10–15).

The automated inversion uses sliding overlapping windows along the data profile. The CPS $C(a,c)$ along the vertical lines related to each window W create a grid of $Q(a,c,u)$ values in depth. The contours of a plotted grid $Q(a,c)$ for a constant parameter u give visual information about the depth of the source. The grids $Q(a,c,u)$ are processed automatically to determine the causative source coordinates and shape. The coordinates (a_m,c_m) and the parameter u_m that minimize Q_m of the estimator of linearity Q determine the position, $x_0 = a_m$ and $z_0 = c_m$, of the characteristic point $M(x_0,z_0)$ and the shape of source through $N = -u_m$. For an ideal-model anomaly of a point source, we have $RSD^*_{min} = 0$ and $Q_m = 0$ (see equations 15 and 17). In the presence of random noise, the RSD^*_{min} approximates the noise standard deviation, as in this case the useful signal in the transform D is a linear function. Deviations of the data from the ideal interpretation model also cause deviations of Q_m from the ideal zero value.

An effective implementation of the described method requires the selection of optimal parameters. As for any inversion technique, reliable results can be expected if the regular data grid has a spacing in the x-direction less than approximately one-third of the depth to the source and a size at least two to three times the source depth. The horizontal spacing of the assigned CPS grid follows the data spacing, while the vertical spacing should be less than this spacing for a more detailed depth determination. The vertical size of the CPS grid has to be sufficiently large so that it can include the characteristic source points. The choice of u corresponds to a choice of the structural index N. It can be taken as an integer $(0, -1,$ and $-2)$ or as a series of real numbers between 0 and -2 in the 2D inversions.

The window length ω is a parameter whose choice depends on the source depth h_s and the number of profile data points. The tests carried out for the dependence of ω on the depth for different parameter values u for the model of a thin dike are represented in Table 1. For the true value of $(-u) = 1$, the minima Q_m obtain their lowest values, while for the other two values of u they are two orders higher. The ratio between Q_m for different parameters u shows the highest value for $\omega = 2h_s$. For this relative window length, the confidence in the determined source type is higher. If the data spacing is equal to $h_s/3$, then the minimum required number of points within the window is seven.

The height of the second data level is also a parameter related mainly to the depth of the source. The synthetic tests show (Figure 9) that the continuation height should be less than or equal to the expected source depth because for a height greater than the source depth, the minima of Q for different parameter values u merge. The well-known amplification of the interference between close anomalies with the upward analytical continuation dictates the use of low second data levels. But a height too low reduces the advantage of using analytical continuations. An acceptable height lies around the half-depth of the source.

The presence of random noise in the data also hinders the shape inversion. An effective suppression of the high wavenumber noise can be achieved by using intermediate levels of analytical continua-

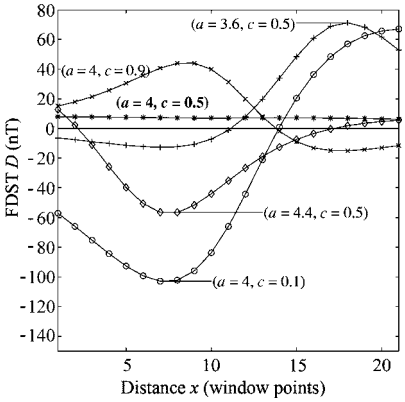

Figure 6. FDST curves D within one window for a dike model with large depth extent with coordinates of the top ($x_0 = 4$ km, $z_0 = 0.5$ km) (see Figure 4) with an added linear background $\Phi = 20 + 5x$ for different CPS $C(a,c) = [(3.6,0.5),(4,0.5),(4,0.9),(4.4,0.5),(4,0.1)]$ km. The 21-point window, point spacing $dx = 0.1$ km, is centered over the respective CPS.

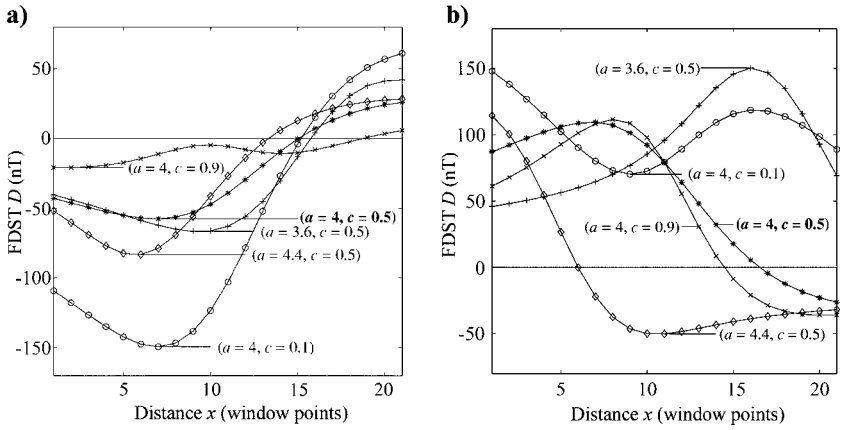

Figure 7. FDST curves D for a dike model with large depth extent (see Figure 4) with coordinates of the top ($x_0 = 4$ km, $z_0 = 0.5$ km) assuming wrong structural indices (a) $N = 2(u = -2)$ and (b) $N = 0(u = 0)$ for different CPS $C(a,c) = [(3.6,0.5),(4,0.5),(4,0.9),(4.4,0.5),(4,0.1)]$ km. The 21-point window, point spacing $dx = 0.1$ km, is centered above the respective CPS.

tion. Results from model tests for different signal-to-noise ratio equal to σ_d/σ_n, where σ_d and σ_n are the standard deviations of the data and the pseudorandom Gaussian noise, respectively, are presented in Table 2. For the true value of the parameter $u = -1$, the improvement of the inversion results with the increase of the intermediate heights is a well-outlined tendency even for the very low value of SNR 10 (zero mean and σ_n = 0.73 nT, 3% of the anomaly amplitude, Gaussian noise). Absolutely confident results for the structural index are obtained for signal-to-noise ratios as low as 30 (σ_n = 0.24 nT, 1% of the anomaly amplitude) for the intermediate continuation level z_1 = 3 km. The accuracy of the estimations for the horizontal and the vertical coordinates of the singular point is almost the same.

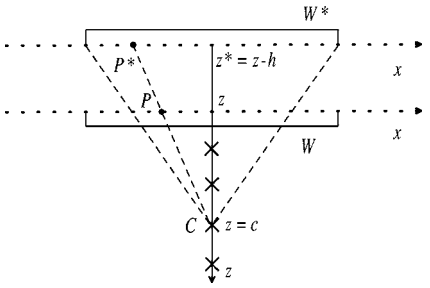

Figure 8. Similarity transformation of the data within the window W at level z to the analytical continuation level at $z^* = z - h$ within the window W^* from a probe point C at a depth $z = c$.

Table 1. Minima Q_m of the linearity estimator Q for different relative window lengths ω, and parameter values $(-u) = N$(structural index) for the model of a thin dike (N= 1) at a depth h_s.

ω	$Q_m(N=1)$	$Q_m(N=2)$	$\frac{Q_m(N=2)}{Q_m(N=1)}$	$Q_m(N=0)$	$\frac{Q_m(N=0)}{Q_m(N=1)}$
$0.5h_s$	0.003	0.050	16.667	0.062	20.667
$1h_s$	0.003	0.070	23.333	0.086	28.667
$2h_s$	0.003	0.075	25.000	0.139	46.333
$4h_s$	0.005	0.111	22.200	0.142	28.400
$6h_s$	0.008	0.147	18.375	0.152	19.000

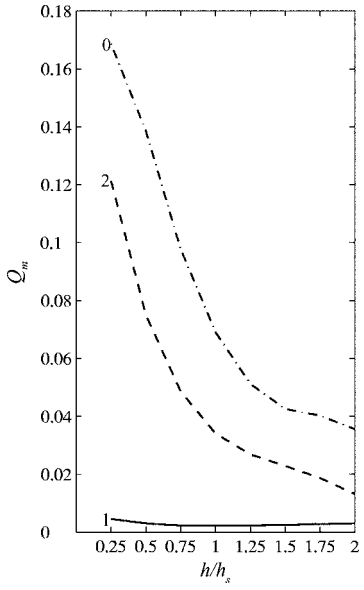

Figure 9. Q_m versus the ratio h/h_s (height of the analytical continuation/depth of the source) for the model of a thin dike (see Figure 11) for structural indices $N = 0, 1, 2$. Window length ω = 17 points.

The inverse operator is sensitive to the magnetic profile curvature. Therefore, for a local magnetic anomaly, the resultant contour map of the linearity estimator Q may contain several local minima. One of them is the global minimum, corresponding to the source position. The others are artificial peripheral minima that are identified and evaluated by their comparative value and position during automatic processing. The elimination of such minima is based on an independent indicator of the source horizontal location, the magnitude magnetic anomaly MMA $T_a (T_a = (H_{a^2} + Z_{a^2})^{1/2}$, where H_a and Z_a are the horizontal and vertical magnetic field components, calculated from TMA data), whose maximum for 2D sources is exactly centered above the source for any magnetization vector direction (Stavrev and Gerovska, 2000). Thus, the Q minima that coincide at or are a small distance from the T_a maxima are accepted, and the distant ones are discarded. The structural index that produces a global minimum with a minimum value of Q is the correct one for the respective local anomaly.

Even though the Q map proposed here is a suitable image of the inverse result, in practice many local anomalies appear within one profile when automatic inversion is to be done over long profiles. To extend the problem beyond an isolated anomaly, we deal with it in a fully automatic way.

We calculate the transform T_a over the whole profile and find all its maxima. We analytically continue the magnetic anomaly to the chosen height over the whole profile. We calculate the function Q for a series of structural index values N. Then, for each Q_N matrix corresponding to a structural index N, we find all local minima using the following procedure. First, we slide a quadratic window $W_n \times W_n$ (W_n is an odd number; in all synthetic and field examples we use W_n = 5) along all probe points of Q_N in x- and z-directions. We find the minimum of Q_N within the window; if the minimum is in the window center, we choose this center as a candidate for a local minimum. Second, we group the points which are candidates for local minima with index Hamming distances less than or equal to $(W_n - 1)/2$; from the minima in each group, we choose the one with a minimal Q_N value. Third, we check for local minima with the same horizontal coordinate a but different vertical coordinates c. From each group, we choose the minimum with the smallest Q_N. Then we narrow the candidates for source locations from all local minima of Q_N for each N. We accept those that are less than a distance L_n from a maximum of T_a and we reject the remaining ones. We repeat the procedure for all N values.

Once the a-, c-coordinates and Q_N of all candidate sources for all N values are obtained, we choose the ones with the correct N. We group all minima for all structural index values according to the horizontal distance from the T_a maxima (found with the same procedure as the minima of Q). Those within a horizontal distance L_n, $L_n = (W_n - 1)/2$ form a group. From the group members, we choose the point with the minimum Q value. The structural index N corresponding to this point defines the shape of the source. The coordinates of the point define the source position.

Thus, we estimate the location and shape of the 2D sources without visual inspection of maps. We only choose a small number of parameters before running the fully automated procedure.

SYNTHETIC MODELS

Figures 10–12 show results from the FDST technique for the three main models of point sources in two dimensions: a thick contact, a dike, and a horizontal cylinder. To illustrate the new method in this article, we draw isovalue maps of Q for each N, presented in a vertical cross section. All the local minima found with the automatic procedure described above are drawn with circles. The circles of the discarded minima are marked with crosses. Thus, the circles without crosses are the chosen minima. We should note the presence of some artifact minima from flaws in the contouring algorithm in the isovalue Q maps not chosen as minima by the automatic procedure. Such examples show that relying on visual inspection does not always produce reliable results. It backs up the necessity of the automatic procedure (described in the Method section) for determining the minima of Q.

The minimum value Q_m of the estimator Q (equation 17) for the three models coincides with the characteristic source point M when the parameter $-u = N$ corresponds to the source shape. If a wrong value is prescribed for N, then Q_m increases (Figure 11). Q_m is estimated precisely in a detailed grid of CPS or by a polynomial approximation using the Q field around the minimal value point. The proposed inversion method works well in the case of neighboring anomalies of two sources with reverse and normal magnetization (see Figure 13).

FIELD EXAMPLES

The new technique was applied to magnetic data from the shelf zone of the Black Sea of southeast Bulgaria, where more than 10 directional anomalies striking west-northwest–east-southeast are observed (Stavrev and Gerovska, 2000). A profile across one of the strongest anomalies just to the east of the town of Nessebar is shown

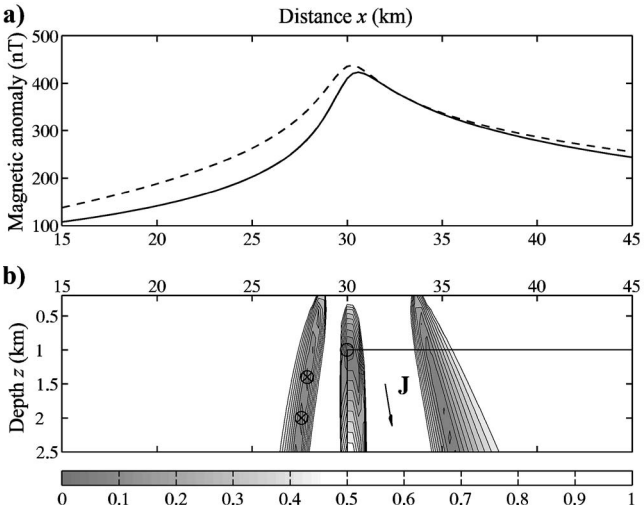

Figure 10. (a) TMA $\Delta T(-)$ and the MMA transform $T_a(--)$ of a thick contact (x_0 = 30 km, z_0 = 1 km, $I_0 = 60°$, J = 0.5 A/m, $D_p = 0$). (b) Contour map of the estimator of linearity Q for the true $N = 0$. Estimated source coordinates (30 km, 1 km), Q_m = 0.002. Window length ω = 7 points, profile spacing dx = 0.3 km. The circles show all the minima candidates. The crosses mark the rejected candidates. Thus, the circle without a cross is the chosen minimum.

Table 2. Results from the FDST inversion, $(\bar{a}_m \pm \sigma_{a_m}, \bar{c}_m \pm \sigma_{c_m})\bar{Q}_m \pm \sigma_{Q_m}$, of the magnetic data with added noise for the model of a thin dike (top at point M(50 km,8 km) and infinite depth extent, see Figure 11) with and without continuing the data to intermediate levels z_1, km. The second continuation level is at $z^* = 4$ km. The window length $\omega = 17$ points, the profile spacing dx = 1 km. $\bar{a}_m$,$\bar{c}_m$, and $\bar{Q}_m$ are the mean values of the estimations for the horizontal position, the depth, and the estimator of linearity; σ_{a_m},σ_{c_m}, and σ_{Q_m} are the standard deviations of the respective estimations for 200 simulations per case of added pseudorandom Gaussian noise. The estimations were made for signal-to-noise ratios σ_d/σ_n = 40,30,20,10 (σ_n = 0.18,0.24,0.36,0.73 nT); σ_d and σ_n are the standard deviations of the magnetic data and the noise, respectively.

SNR	N	$z_1 = 0$	$z_1 = 1$ km	$z_1 = 2$ km	$z_1 = 3$ km
	1	(49.4±0.8,7.6±0.5) 0.12±0.02	(50.0±0.2,8.0±0.2) 0.07±0.02	(50.0±0.0,8.0±0.1) 0.05±0.02	(50.0±0.0,8.0±0.0) 0.04±0.02
40	2	(49.2±0.5,11.1±0.4) 0.12±0.02	(49.5±0.5,11.5±0.5) 0.09±0.02	(49.5±0.5,11.8±0.4) 0.10±0.02	(49.4±0.5,12.0±0.2) 0.12±0.02
	0	(48.8±1.2,4.0±0.3) 0.14±0.04	(49.9±0.7,4.1±0.3) 0.13±0.03	(50.2±0.4,4.2±0.4) 0.13±0.02	(50.3±0.5,4.3±0.5) 0.15±0.02
	1	(49.1±0.7,7.2±0.4) 0.14±0.04	(50.0±0.1,7.9±0.2) 0.08±0.02	(50.0±0.2,7.9±0.4) 0.07±0.02	(50.0±0.1,8.0±0.0) 0.06±0.02
30	2	(49.0±0.6,11.0±0.3) 0.14±0.02	(49.4±0.5,11.4±0.5) 0.11±0.02	(49.5±0.5,11.7±0.4) 0.10±0.02	(49.4±0.5,12.0±0.3) 0.12±0.02
	0	(48.5±1.1,3.9±0.4) 0.15±0.04	(49.8±0.9,4.1±0.6) 0.13±0.03	(50.3±0.4,4.3±0.5) 0.13±0.02	(50.3±0.5,4.2±0.5) 0.14±0.02
	1	(48.6±0.9,7.1±0.6) 0.17±0.04	(49.7±0.6,7.8±0.6) 0.11±0.03	(49.9±0.4,7.9±0.4) 0.09±0.03	(49.9±0.3,7.9±0.3) 0.08±0.03
20	2	(48.6±0.8,10.8±0.6) 0.19±0.04	(49.4±0.5,11.5±0.5) 0.12±0.03	(49.5±0.5,11.7±0.5) 0.11±0.03	(49.5±0.5,11.9±0.5) 0.11±0.03
	0	(48.2±1.1,3.6±0.6) 0.18±0.04	(49.7±1.1,4.1±0.6) 0.13±0.03	(50.2±0.7,4.1±0.6) 0.13±0.03	(50.3±0.6,4.1±0.7) 0.14±0.03
	1	(48.4±1.6,6.3±1.1) 0.25±0.06	(49.0±1.1,7.2±0.7) 0.16±0.05	(49.5±0.9,7.6±0.7) 0.14±0.04	(49.7±0.7,7.8±0.7) 0.13±0.04
10	2	(49.0±2.4,9.5±1.6) 0.30±0.08	(48.9±0.9,11.1±0.8) 0.18±0.06	(49.3±0.8,11.6±0.8) 0.16±0.06	(49.4±0.6,11.8±0.7) 0.15±0.05
	0	(47.8±1.4,3.5±0.6) 0.23±0.07	(48.9±1.5,3.6±0.6) 0.16±0.05	(49.6±1.3,3.8±0.8) 0.15±0.05	(50.1±1.0,3.9±0.8) 0.14±0.04

in Figure 14a. The Q plot forms a minimal value $Q_m = 0.21$ at a depth of 0.8 km for the parameter $u = -1$, i.e., for the structural index $N = 1$ (Figure 14b). For $u = -2$ ($N = 2$), Figure 14c, the Q map produces a higher value for the minimum $Q_m = 0.30$ at a depth of 1.4 km. This means that the source is close to the dike model, but the comparatively low value of Q_m for $N = 2$ indicates a source with a limited depth extent.

As a second field example, we use here an aeromagnetic profile over a known dike published by Keating and Pilkington (2004). We have digitized the TMA at a spacing of 10 m (Figure 15a). The analytical continuation to 50 m above the level of measurements is calculated, and FDST analysis carried out using overlapping 41-point windows. The results are shown in Figure 15b and in Table 3. The minimum value of the Q-estimator appears at a depth of 126 m below the level of the magnetic sensor, or 53 m below the ground surface for a structural index. This result indicates a dike as the source of the interpreted anomaly. The estimated depth is close to the known depth of about 41 m (Keating and Pilkington, 2004).

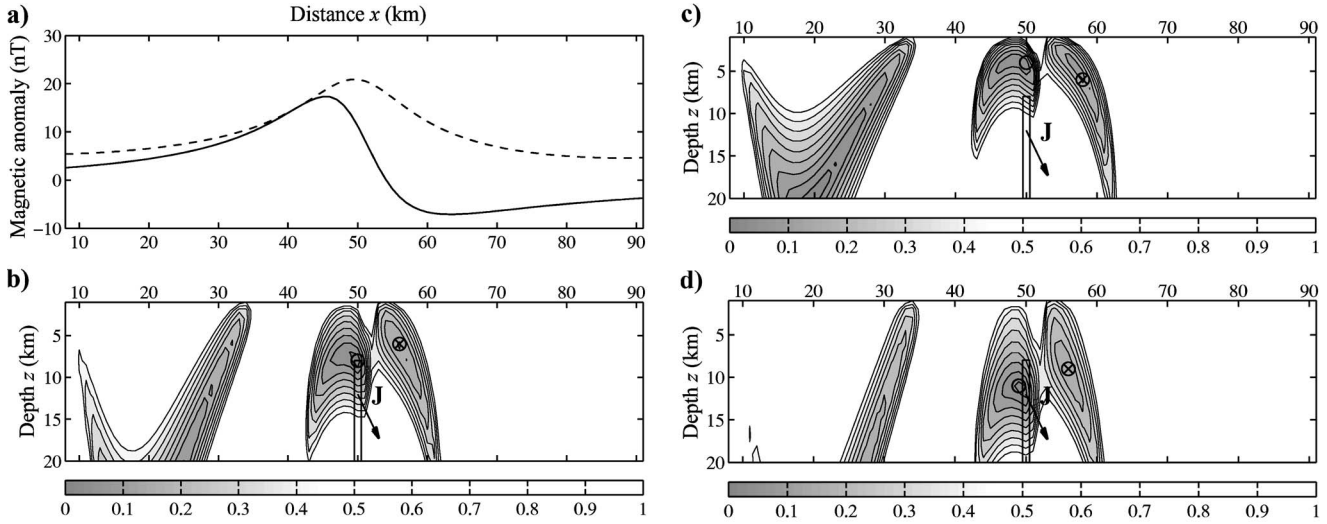

Figure 11. (a) TMA $\Delta T(-)$ and the transform MMA $T_a(--)$ for a dike model ($x_0 = 50$ km, $z_0 = 8$ km, $I_0 = 60°$, $D_0 = 0$, $J = 1$ A/m, $D_p = 0$). Contour maps of the estimator of linearity Q for (b) $N = 1$. Estimated source coordinates (50 km, 8 km), $Q_m = 0.003$. (c) $N = 0$. Estimated source coordinates (50 km, 4 km), $Q_m = 0.139$. (d) $N = 2$. Estimated source coordinates (49 km,11 km), $Q_m = 0.075$. Window length $\omega = 17$ points, profile spacing $dx = 1$ km. The circles show all the minima candidates. The crosses mark the rejected candidates. Thus, the circles without a cross are the chosen minima.

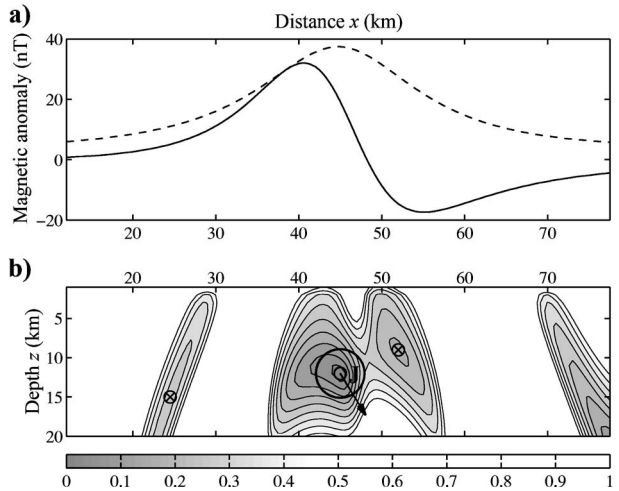

Figure 12. (a) TMA $\Delta T(-)$ and the MMA transform $T_a(--)$ of a horizontal cylinder model ($x_0 = 45$ km, $z_0 = 12$ km, $I_0 = 60°$, $J = 1$ A/m, $D_p = 0$). (b) Contour map of the estimator of linearity Q for the true $N = 2$. The estimated source coordinates are (45 km, 12 km), $Q_m = 0.007$. [For $N = 1$, coordinates (45.5 km,8 km), $Q_m = 0.072$; for $N = 0$, coordinates (46 km, 5 km), $Q_m = 0.116$.] Window length $\omega = 49$ points, profile spacing $dx = 0.5$ km. The circles show all the minima candidates. The crosses mark the rejected candidates. Thus, the circle without a cross is the chosen minimum.

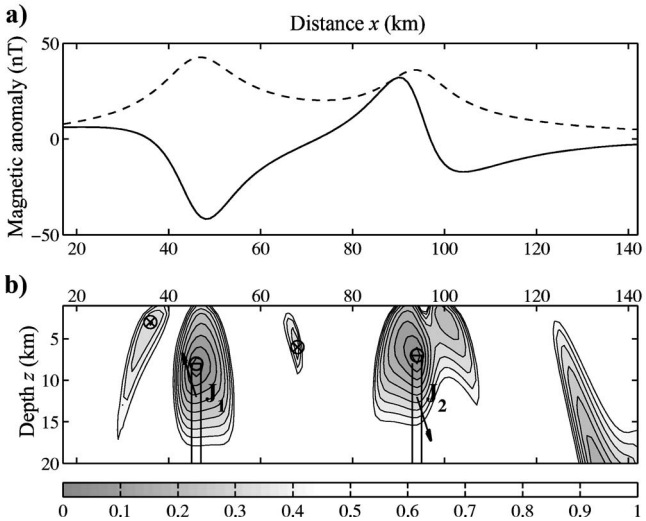

Figure 13. (a) TMA $\Delta T(-)$ and the MMA transform $T_a(--)$ of two dikes ($J_1 = J_2 = 1$ A/m, $I_1 = -60°$, $I_2 = 60°$, $D_1 = 180°$, $D_2 = 0$, $D_p = 0$) with coordinates of the tops (46 km,8 km) and (94 km,7 km). (b) Contour map of the estimator of linearity Q for the true $N = 1$. The estimated source coordinates are (46 km,8 km), $Q_m = 0.048$, and (94 km,7 km), $Q_m = 0.014$. Window length $\omega = 49$ points, profile spacing $dx = 0.5$ km. The circles show all the minima candidates. The crosses mark the rejected candidates. Thus, the circles without a cross are the chosen minima.

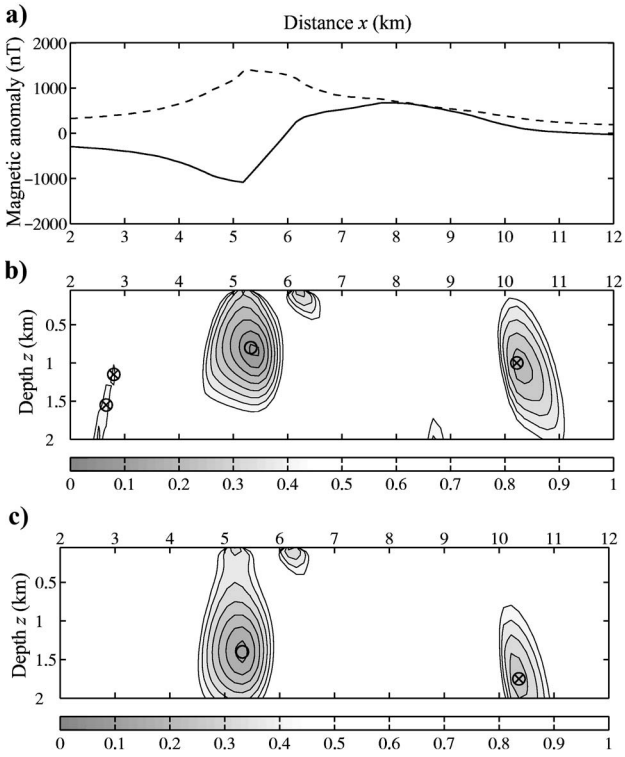

Figure 14. Field example from the southeast Bulgaria Black Sea shelf. (a) TMA $\Delta T(-)$ and the MMA transform $T_a(--)$. Contour maps of the estimator of linearity Q for (b) $N = 1$. Estimated source coordinates $x_0 = 5.3$ km, $z_0 = 0.8$ km, $Q_m = 0.21$. (c) $N = 2$. Estimated source coordinates $x_0 = 5.3$ km, $z_0 = 1.4$ km, $Q_m = 0.30$. The circles show all minima candidates. The crosses mark the rejected candidates. Thus, the circles without a cross are the chosen minima.

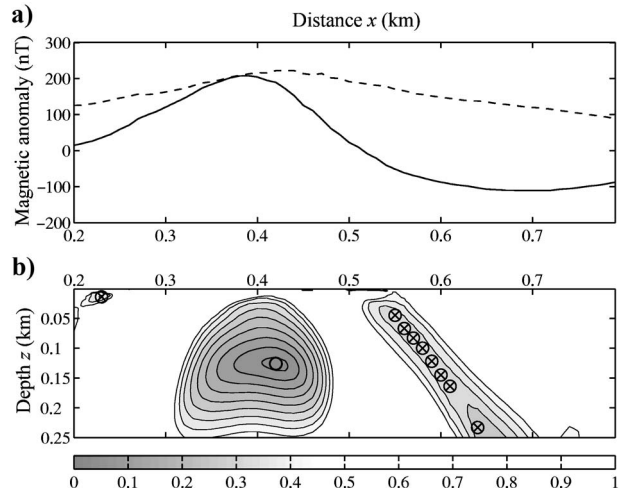

Figure 15. Field example after Keating and Pilkington (2004). (a) TMA $\Delta T(-)$ and the MMA transform $T_a(--)$. (b) Contour map of the estimator of linearity Q for $N = 1, Q_m = 0.069$. The estimated source coordinates are $x_0 = 420$ m, $z_0 = 126$ m (depth equal to 53 m from the ground surface) (see also Table 3). The circles show all minima candidates. The crosses mark the rejected candidates. Thus, the circle without a cross is the chosen minimum.

Table 3. Results from the FDST inversion of the magnetic data in Figure 15. (x_0,z_0) are the estimated horizontal and vertical coordinates of the source; d is the depth from the ground of the source. Q_m denotes the minimal value of the linearity estimator Q.

$N = -u$	x_0 (m)	z_0 (m)	d (m)	Q_m
0	410	200	127	0.136
1	420	126	53	0.069
2	420	57	−16	0.093

CONCLUSIONS

We have proposed a new automatic technique for inversion of magnetic data based on the homogeneity property of potential fields. The principal definition of a homogeneous function is applied instead of Euler's differential equation. This alternative approach allows the construction of an inverse operator using only the measured magnetic data and their upward analytical continuation. The latter contributes to the stability of the solution in the presence of high-wavenumber noise. This gives an advantage to the proposed method in comparison with techniques using first- and higher-order derivatives. The inverse operator does not include the solution of a system of equations like the conventional Euler deconvolution, whose stability is also a problem because of the high correlation coefficient between the measured field and its vertical derivative. A detailed analysis shows the utility of the finite-difference similarity transform based on the principal definition of homogeneity. The inverse results can be obtained in terms of depth and shape of simple sources in the presence of constant or linear background and significant random noise. The inverse procedures allow full automatization. Two main parameters control the inversion parameter, the height of the analytical continuation, and the window length. Those can be estimated by the width of the local anomalies. The density of the probe grid in the downward hemispace and a tolerance for the estimations of the source location around the anomaly magnitude maximum are additional parameters. The fully automated output is given in numerical form and auxiliary plot.

The proposed method can also be applied for the inversion of gravity data, as well as gravity and magnetic gradiometric data.

ACKNOWLEDGMENTS

We are grateful to the editor, J. B. C. Silva, for his valuable comments. We also thank the reviewers for their useful remarks. M. J. Araúzo-Bravo recognizes the Japanese Society for the Promotion of Science for supporting him in this research.

REFERENCES

Barbosa, V. C. F., J. B. C. Silva, and W. E. Medeiros, 1999, Stability analysis and improvement of structural index estimation in Euler deconvolution: Geophysics, **64**, 48–60.

Courant, R., and F. John, 1965, Introduction to calculus and analysis: Wiley Interscience.

Dimitrov, L., and P. Stavrev, 1968, On the determination of systematical errors at the method of similar abscissas: Academie Bulgare des Sciences, Bulletin de l'Institute de Geophysique, **13**, 177–194.

Gellert, W., H. Kastner, and S. Neuber, 1979, Lexikon der mathematik: VEB Bibliographisches Inst.

Gerovska, D., and M. J. Araúzo-Bravo, 2003, Automatic interpretation of magnetic data based on Euler deconvolution with unprescribed structural index: Computers and Geosciences, **29**, 949–960.
Gerovska, D., P. Stavrev, and M. J. Araúzo-Bravo, 2005, Finite-difference Euler deconvolution algorithm applied for interpretation of magnetic data from northern Bulgaria: Pure and Applied Geophysics, **162**, 591–608.
Hsu, S. K., 2002, Imaging magnetic sources using Euler's equation: Geophysical Prospecting, **50**, 15–25.
Keating, P., and M. Pilkington, 2004, Euler deconvolution of the analytic signal and its application to magnetic interpretation: Geophysical Prospecting, **52**, 165–182.
Martelet, G., P. Sailhac, F. Moreau, and M. Diament, 2001, Characterization of geological boundaries using 1-D wavelet transform on gravity data: Theory and application to the Himalayas: Geophysics, **66**, 1116–1129.
Mikhailov, V., A. Galdeano, M. Diament, A. Gvishiani S. Agayan, S. Bogoutdinov, E. Gravea., and P. Sailhac, 2003, Application of artificial intelligence for Euler solutions clustering: Geophysics, **68**, 168–180.
Moreau, F., D. Gilbert, M. Holschneider, and G. Saracco, 1997, Wavelet analysis of potential fields: Inverse Problems, **13**, 165–178.
Ravat, D., 1996, Analysis of the Euler method and its applicability in environmental investigations: Journal of Environmental and Engineering Geophysics, **1**, 229–238.
Reid, A. B., 1995, Euler deconvolution: Past, present, and future — A review: 65th Annual International Meeting, SEG, Expanded Abstracts, 272–273.
Reid, A. B., J. M. Allsop, H. Granser, A. J. Millett, and I. W. Somerton, 1990, Magnetic interpretation in three dimensions using Euler deconvolution: Geophysics, **55**, 80–91.
Sailhac, P., and D. Gibert, 2003, Identification of sources of potential fields with the continuous wavelet transform: Journal of Geophysical Research, **108**, 2296–2306.
Slack, H. A., V. M. Lynch, and L. Langan, 1967, The geomagnetic gradiometer: Geophysics, **32**, 877–892.
Stavrev, P. Y., 1997, Euler deconvolution using differential similarity transformations of gravity or magnetic anomalies: Geophysical Prospecting, **45**, 207–246.
Stavrev, P., and D. Gerovska, 2000, Magnetic field transforms with low sensitivity to the direction of source magnetization and high centricity: Geophysical Prospecting, **48**, 317–340.
Telford, W. M., L. P. Geldart, and R. E. Sheriff, 1990, Applied geophysics: Cambridge Univ. Press.
Thompson, D. T., 1982, EULDPH — A new technique for making computer-assisted depth estimates from magnetic data: Geophysics, **47**, 31–37.
Tikhonov, A. N., and V. I. Arsenin, 1977, Solution of ill-posed problems: V. H. Winston and Sons.
Valée, M. A., P. Keating., R. S. Smith, and C. St.-Hilaire, 2004, Estimating depth and model type using continuous wavelet transform of magnetic data: Geophysics, **69**, 191–199.